Fabrication and characterization of polycarbonate microstructured polymer optical fibers for high-temperature-resistant fiber Bragg grating strain sensors

Andrea Fasano,[1] Getinet Woyessa,[2] Pavol Stajanca,[3] Christos Markos,[2,4] Alessio Stefani,[2,5] Kristian Nielsen,[2] Henrik K. Rasmussen,[1] Katerina Krebber,[3] and Ole Bang[2,*]

[1] *DTU Mekanik, Department of Mechanical Engineering, Technical University of Denmark, 2800 Kgs. Lyngby, Denmark*
[2] *DTU Fotonik, Department of Photonics Engineering, Technical University of Denmark, 2800 Kgs. Lyngby, Denmark*
[3] *Division 8.6 "Optical and Fibre Optic Methods", BAM Federal Institute for Materials Research and Testing, 12205 Berlin, Germany*
[4] *CREOL, The College of Optics & Photonics, University of Central Florida, 4000 Central Florida Blvd., Orlando, FL 32816, USA*
[5] *Institute of Photonics and Optical Science (IPOS), School of Physics, The University of Sydney, NSW 2006, Australia*
[*] *oban@fotonik.dtu.dk*

Abstract: Here we present the fabrication of a solid-core microstructured polymer optical fiber (mPOF) made of polycarbonate (PC), and report the first experimental demonstration of a fiber Bragg grating (FBG) written in a PC optical fiber. The PC used in this work has a glass transition temperature of 145°C. We also characterize the mPOF optically and mechanically, and further test the sensitivity of the PC FBG to strain and temperature. We demonstrate that the PC FBG can bear temperatures as high as 125°C without malfunctioning. In contrast, polymethyl methacrylate-based FBG technology is generally limited to temperatures below 90°C.

OCIS codes: (060.2370) Fiber optics sensors; (060.3735) Fiber Bragg gratings; (060.4005) Microstructured fibers; (060.2270) Fiber characterization; (160.5470) Polymers.

References and links

1. D. J. Webb, "Polymer Fiber Bragg Grating Sensors and Their Applications," in *Optical Fiber Sensors: Advanced Techniques and Applications*, G. Rajan, ed. (CRC Press, 2015).
2. K. Peters, "Polymer optical fiber sensors — a review," Smart Mater. Struct. **20**(1), 013002 (2011).
3. Cambridge University Engineering Department, *Materials Data Book*, (Cambridge University Engineering Department, 2003), http://www-mdp.eng.cam.ac.uk/web/library/enginfo/cueddatabooks/materials.pdf.
4. J. Jensen, P. Hoiby, G. Emiliyanov, O. Bang, L. Pedersen, and A. Bjarklev, "Selective detection of antibodies in microstructured polymer optical fibers," Opt. Express **13**(15), 5883–5889 (2005).
5. G. Emiliyanov, J. B. Jensen, O. Bang, P. E. Hoiby, L. H. Pedersen, E. M. Kjaer, and L. Lindvold, "Localized biosensing with Topas microstructured polymer optical fiber," Opt. Lett. **32**(5), 460–462 (2007).
6. G. Emiliyanov, P. E. Høiby, L. H. Pedersen, and O. Bang, "Selective serial multi-antibody biosensing with TOPAS microstructured polymer optical fibers," Sensors (Basel) **13**(3), 3242–3251 (2013).
7. H. U. Hassan, K. Nielsen, S. Aasmul, and O. Bang, "Polymer optical fiber compound parabolic concentrator tip for enhanced coupling efficiency for fluorescence based glucose sensors," Biomed. Opt. Express **6**(12), 5008–5020 (2015).
8. G. D. Peng, Z. Xiong, and P. L. Chu, "Photosensitivity and gratings in dye-doped polymer optical fibers," Opt. Fiber Technol. **5**(2), 242–251 (1999).
9. Z. Xiong, G. D. Peng, B. Wu, and P. L. Chu, "Highly tunable Bragg gratings in single-mode polymer optical fibers," IEEE Photonics Technol. Lett. **11**(3), 352–354 (1999).
10. W. Zhang, A. Abang, D. J. Webb, and G.-D. Peng, "Wavelength Drift of PMMA-Based Optical Fiber Bragg Grating Induced by Optical Absorption," IEEE Photonics Technol. Lett. **27**(4), 336–339 (2015).
11. A. Lacraz, M. Polis, A. Theodosiou, C. Koutsides, and K. Kalli, "Femtosecond Laser Inscribed Bragg Gratings in Low Loss CYTOP Polymer Optical Fiber," IEEE Photonic. Tech. L. **27**(7), 693–696 (2015).

#255045 Received 3 Dec 2015; revised 15 Jan 2016; accepted 17 Jan 2016; published 27 Jan 2016

12. I. P. Johnson, W. Yuan, A. Stefani, K. Nielsen, H. K. Rasmussen, L. Khan, D. J. Webb, K. Kalli, and O. Bang, "Optical fibre Bragg grating recorded in TOPAS cyclic olefin copolymer," Electron. Lett. **47**(4), 271–272 (2011).
13. W. Yuan, L. Khan, D. J. Webb, K. Kalli, H. K. Rasmussen, A. Stefani, and O. Bang, "Humidity insensitive TOPAS polymer fiber Bragg grating sensor," Opt. Express **19**(20), 19731–19739 (2011).
14. C. Markos, A. Stefani, K. Nielsen, H. K. Rasmussen, W. Yuan, and O. Bang, "High-Tg TOPAS microstructured polymer optical fiber for fiber Bragg grating strain sensing at 110 degrees," Opt. Express **21**(4), 4758–4765 (2013).
15. M. van Eijkelenborg, M. Large, A. Argyros, J. Zagari, S. Manos, N. Issa, I. Bassett, S. Fleming, R. McPhedran, C. M. de Sterke, and N. A. P. Nicorovici, "Microstructured polymer optical fibre," Opt. Express **9**(7), 319–327 (2001).
16. J. C. Knight, T. A. Birks, P. S. J. Russell, and D. M. Atkin, "All-silica single-mode optical fiber with photonic crystal cladding," Opt. Lett. **21**(19), 1547–1549 (1996).
17. M. C. J. Large, L. Poladian, G. W. Barton, and M. A. van Eijkelenborg, *Microstructured Polymer Optical Fibres* (Springer, 2008).
18. A. Argyros, "Microstructures in Polymer Fibres for Optical Fibres, THz Waveguide, and Fibre-Based Metamaterials," ISRN Optics. 785162 (2013).
19. M. A. van Eijkelenborg, A. Argyros, and S. G. Leon-Saval, "Polycarbonate hollow-core microstructured optical fiber," Opt. Lett. **33**(21), 2446–2448 (2008).
20. J. Harrington, R. George, P. Pedersen, and E. Mueller, "Hollow polycarbonate waveguides with inner Cu coatings for delivery of terahertz radiation," Opt. Express **12**(21), 5263–5268 (2004).
21. G. T. T. Gibson, R. D. Wright, and R. D. Oleschuk, "Multiple electrosprays generated from a single polycarbonate microstructured fibre," J. Mass Spectrom. **47**(3), 271–276 (2012).
22. Y. Gao, N. Guo, B. Gauvreau, M. Rajabian, O. Skorobogata, E. Pone, O. Zabeida, L. Martinu, C. Dubois, and M. Skorobogatiy, "Consecutive Solvent Evaporation and Co-Rolling Techniques for Polymer Multilayer Hollow Fiber Preform Fabrication," J. Mater. Res. **21**(9), 2246–2254 (2006).
23. T. R. Woliński, M. Tefelska, K. Mileńko, A. Siarkowska, D. Budaszewski, A. W. Domański, S. Ertman, K. Orzechowski, K. Rutkowska, M. Sierakowski, E. Nowinowski-Kruszelnicki, R. Dąbrowski, and P. Mergo, "Photonic Liquid Crystal Fibers with Polymers," Acta Phys. Pol. A **124**(3), 613–616 (2013).
24. Y. Koike, T. Ishigure, and E. Nihei, "High-Bandwidth Graded-Index Polymer Optical Fiber," J. Lightwave Technol. **13**(7), 1475–1489 (1995).
25. A. Tanaka, H. Sawada, T. Takoshima, and N. Wakatsuki, "New plastic optical fiber using polycarbonate core and fluorescence-doped fiber for high temperature use," Fiber Integr. Opt. **7**(2), 139–158 (1988).
26. S. Irie and M. Nishiguchi, "Development of the heat resistant plastic optical fiber," in *Proceedings of the Third International Conference on Plastic Optical Fibres & Applications*, (Yokohama, Japan, 1994), pp. 88–91.
27. O. Ziemman, J. Krauser, P. E. Zamzow, and W. Daum, *POF Handbook. Optical Short Range Transmission Systems* (Springer, 2008), Chap. 2.
28. D. G. Legrand and J. T. Bendler, *Handbook of Polycarbonate Science and Technology* (Marcel Dekker, 2000).
29. Bayer MaterialScience AG, "Optical properties of Makrolon and Apec for non-imaging optics," (Bayer MaterialScience AG, 2014), http://www.plastics.covestro.com/Products/~/media/B6555362438341FF9804F21A253E5B23.ashx?la=en.
30. M. D. Migahed and H. M. Zidan, "Influence of UV-irradiation on the structure and optical properties of polycarbonate films," Curr. Appl. Phys. **6**(1), 91–96 (2006).
31. K. Hareesh, A. K. Pandey, Y. Sangappa, R. Bhat, A. Venkataraman, and G. Sanjeev, "Changes in the properties of Lexan polycarbonate by UV irradiation," Nucl. Instrum. Methods Phys. Res. B **295**, 61–68 (2013).
32. J. Liu, S. Wang, M. Lv, and X. Zeng, "Surface modification of bisphenol A polycarbonate material by ultraviolet Nd:YVO_4 laser high-speed microprocessing technology," J. Micromech. Microeng. **24**(8), 085002 (2014).
33. A. Mockutė, R. Tomašiūnas, R. Petruškevičius, and D. Jucius, "Formation technology of planar polymer waveguide structure," Lith. J. Phys. **47**(4), 411–414 (2007).
34. K. E. Carroll, C. Zhang, D. J. Webb, K. Kalli, A. Argyros, and M. C. J. Large, "Thermal response of Bragg gratings in PMMA microstructured optical fibers," Opt. Express **15**(14), 8844–8850 (2007).
35. A. Son, A. Alizadeh, and H. Marand, "On the multiple melting behavior of bisphenol-A polycarbonate," Polymer (Guildf.) **41**(25), 8879–8886 (2000).
36. B. T. Kuhlmey, R. C. McPhedran, and C. Martijn de Sterke, "Modal cutoff in microstructured optical fibers," Opt. Lett. **27**(19), 1684–1686 (2002).
37. N. Sultanova, S. Kasarova, and I. Nikolov, "Dispersion Properties of Optical Polymers," Acta Phys. Pol. A **116**(4), 585–587 (2009).
38. T. Yamashita and K. Kamada, "Intrinsic Transmission Loss of Polycarbonate Core Optical Fiber," Jpn. J. Appl. Phys. **32**(Part 1, No. 6A), 2681–2686 (1993).
39. T. B. Gorczyca and M.-Y. Shih, "Photo-defined Polymeric Photonic Materials and Processes," Proc. SPIE **5179**, 97–104 (2003).
40. A. Stefani, K. Nielsen, H. K. Rasmussen, and O. Bang, "Cleaving of TOPAS and PMMA microstructured polymer optical fibers: Core-shift and statistical quality optimization," Opt. Commun. **285**(7), 1825–1833 (2012).
41. A. Argyros, R. Lwin, S. G. Leon-Saval, J. Poulin, L. Poladian, and M. C. J. Large, "Low loss and temperature stable microstructured polymer optical fibers," J. Lightwave Technol. **30**(1), 192–197 (2012).

#255045 Received 3 Dec 2015; revised 15 Jan 2016; accepted 17 Jan 2016; published 27 Jan 2016

42. M. A. van Eijkelenborg, A. Argyros, A. Bachmann, G. Barton, M. C. J. Large, G. Henry, N. A. Issa, K. F. Klein, H. Poisel, W. Pok, L. Poladian, S. Manos, and J. Zagari, "Bandwidth and loss measurements of graded-index microstructured polymer optical," Electron. Lett. **40**(10), 592–593 (2004).
43. I.-L. Bundalo, K. Nielsen, C. Markos, and O. Bang, "Bragg grating writing in PMMA microstructured polymer optical fibers in less than 7 minutes," Opt. Express **22**(5), 5270–5276 (2014).
44. T. Wang, Q. Wang, Y. Luo, W. Qiu, G.-D. Peng, B. Zhu, Z. Hu, G. Zou, and Q. Zhang, "Enhancing photosensitivity in near UV/vis band by doping 9-vinylanthracene in polymer optical fiber," Opt. Commun. **307**, 5–8 (2013).
45. D. Sáez-Rodríguez, K. Nielsen, H. K. Rasmussen, O. Bang, and D. J. Webb, "Highly photosensitive polymethyl methacrylate microstructured polymer optical fiber with doped core," Opt. Lett. **38**(19), 3769–3772 (2013).
46. R. Oliveira, L. Bilro, and R. Nogueira, "Bragg gratings in a few mode microstructured polymer optical fiber in less than 30 seconds," Opt. Express **23**(8), 10181–10187 (2015).
47. W. Yuan, A. Stefani, M. Bache, T. Jacobsen, B. Rose, N. Herholdt-Rasmussen, F. K. Nielsen, S. Andresen, O. B. Sørensen, K. S. Hansen, and O. Bang, "Improved thermal and strain performance of annealed polymer optical fiber Bragg gratings," Opt. Commun. **284**(1), 176–182 (2011).
48. C. Jiang, M. G. Kuzyk, J.-L. Ding, W. E. Johns, and D. J. Welker, "Fabrication and mechanical behavior of dye-doped polymer optical fiber," J. Appl. Phys. **92**(1), 4–12 (2002).
49. A. Stefani, W. Yuan, C. Markos, and O. Bang, "Narrow Bandwidth 850-nm Fiber Bragg Gratings in Few-Mode Polymer Optical Fibers," IEEE Photonics Technol. Lett. **23**(10), 660–662 (2011).
50. I. P. Johnson, K. Kalli, and D. J. Webb, "827nm Bragg grating sensor in multimode microstructured polymer optical fibre," Electron. Lett. **46**(17), 1217–1218 (2010).
51. K. Kalli and D. J. Webb, "Polymer Optical Fiber-Based Sensors," in *Advanced Fiber Optics: Concepts and Technology*, L. Thévenaz, ed. (EPFL Press, 2011).
52. B. Crist, "Yield processes in glassy polymers," in *The Physics of Glassy Polymers*, R. N. Haward and R. J. Young, ed. (Springer Science & Business Media, 1997).
53. N. G. McCrum, C. P. Buckley, and C. B. Bucknall, *Principles of Polymer Engineering* (Oxford University Press, 1997), Chap. 5.
54. GEHR GmbH, "Technical Data Sheet – GEHR PMMA ," (GEHR GmbH, 2013), http://www.gehrplastics.com/images/upload/downloads/tech_datenblaetter/acrylic/PMMA_en.pdf.
55. TOPAS Advanced Polymers Inc, "Data Sheet - TOPAS 8007S-04," (TOPAS Advanced Polymers Inc., 2014), http://www.topas.com/sites/default/files/TDS_8007S-04_english%20units_2.pdf.
56. A. Stefani, S. Andresen, W. Yuan, N. Herholdt-Rasmussen, and O. Bang, "High Sensitivity Polymer Optical Fiber-Bragg-Grating-Based Accelerometer," IEEE Photonics Technol. Lett. **24**(9), 763–765 (2012).

1. Introduction

Polymer optical fiber (POF) sensors offer several advantages over their silica-based counterpart. First of all, POFs have a larger strain range available and an increased sensitivity to stress due to a considerably lower Young's modulus [1,2]. Young's modulus is in the range 68-74 GPa for silica glass, 2.2-3.8 GPa for polymethyl methacrylate (PMMA), and 2.0-2.4 GPa for polycarbonate (PC) [3]. Because of their biocompatibility, flexibility in bending, and non-brittle nature, POFs represent ideal candidates for in-vivo biosensing applications [4–7]. Another attractive characteristic of POFs lies in the possibility to detect different chemical and biochemical species by changing functional groups, polymerization process, and additives, since they are made of organic compounds [1]. In addition, polymers have lower density than silica glass [3], which is in general desirable, as it is often necessary to minimize the total weight of a device. The aforementioned characteristics come in handy especially in fiber Bragg grating (FBG) sensors, for some applications of which, materials alternative to silica are incessantly sought for. To date, the most widespread material for polymer-based FBGs is PMMA [1,2,8–10], although the use of some alternative plastics, such as CYTOP (amorphous fluoropolymer) [11] and TOPAS (cyclic olefin copolymer) [12–14], has recently been investigated.

Microstructured polymer optical fibers (mPOFs) have drawn increasing attention since 2001 [15], within the framework of the research on photonic crystal fibers starting in the 1990s [16], due to the large variety of optical effects obtainable simply by changing internal microstructure [17,18]. In this class of fibers, the ability to guide light is based on a patterning of microscopic holes running along the length of a fiber [15–18]. Only a few journal papers on mPOFs made of PC have been published to date. None of those papers, however, have demonstrated light propagation in a solid-core microstructured PC fiber. Van Eijkelenborg et al. [19] fabricated and characterized a hollow-core PC mPOF fiber, where the polymer preform was produced via capillary stacking technique. Hollow-core PC waveguides with inner Cu coatings were employed in [20] for terahertz transmission, while Gibson et al. [21] made use of solid-core PC mPOFs to fabricate multichannel electrospray emitters. Moreover, PC was studied in combination with polyvinyl difluoride (PVDF) for the manufacturing of mPOFs from multilayered all-polymer hollow preforms prepared by solvent evaporation and co-rolling methods [22]. A PC mPOF was further reported in [23], where, however, localized light propagation in the core could not be achieved (the light source was a 633-nm laser).

Polycarbonate optical fibers were introduced by Fujitsu in 1986 (the core was made of PC, with a polyolefin-based material as the cladding) [24] and have been extensively studied and used since then [25–27]. Polycarbonate is an engineering plastic that exhibits excellent clarity and impact strength [28]. The main advantage of using this material for optical fiber fabrication indeed lies in the well-balanced combination of its optical and mechanical properties. Firstly, it is transparent to visible light [29] and for this reason can be considered as a natural alternative to PMMA. Secondly, PC usually yields and breaks at elevated values of strain [29], and is highly flexible in bending. In addition, its glass transition temperature (T_g) is one of the highest among transparent plastics, thereby resulting in a larger available temperature range. These properties make PC fibers particularly attractive for those applications requiring high-temperature-resistant polymer sensors, as long as the specific application does not involve long-term exposure to a high-humidity environment at high temperature. Early investigations indeed seem to indicate that humid heat may cause premature aging of PC POFs [27].

The change of properties in PC due to UV irradiation has been the subject of several studies [30–32]. In particular, photosensitivity studies on PC [30] showed that the refractive index profile of PC films was affected by UV irradiation, suggesting a potential applicability of the photo-irradiation dependency for optical devices. Nevertheless, to the best of our knowledge, no FBG in PC optical fibers has been demonstrated yet. Literature only reports the inscription of Bragg gratings into a PC-based planar waveguide via an ablation process [33]. Here we present the first experimental demonstration of an endlessly single-mode solid-core PC mPOF. The microstructured fiber, fabricated via mechanical casting from plastic granulates, is also characterized both optically and mechanically. We further write an FBG into the optical fiber (which is dopant-free) by using a UV laser and demonstrate strain sensing up to 3%, and a linear response to temperature up to the record of 125°C with neither malfunctioning nor any significant hysteresis in the cooling phase. Microstructured polymer optical fiber Bragg gratings (mPOFBGs) made of a high-T_g grade of TOPAS (5013) were previously tested up to 110°C [14], whilst the maximum operation temperature of PMMA was reported to be 92°C in [34]. We consider the present work as a further step towards enabling high-temperature-resistant POFBG technology.

2. Experimental results

2.1 Fabrication of the solid-core PC mPOF

The solid-core PC mPOF was fabricated by using a drill-and-draw technique starting from casting of plastic granulates. The material used for casting was Makrolon LED2245 from Bayer MaterialScience AG with a T_g of 145°C. This material grade shows an extremely low tendency towards yellowing, even at temperatures as high as 120 °C [29]. Being hygroscopic, the PC granulates needed to be dried before casting to avoid bubble formation, which would otherwise increase the transmission loss and degrade the mechanical properties of the final fiber. A strict control of timing, temperature, and pressure was also required during the casting in order to obtain a good-quality solid rod. In particular, relatively high temperatures were applied as PC might contain polymer crystals at temperatures even higher than 220°C [35]. The presence of residual crystals in the PC preform would lead to both considerably poorer optical performance and inhomogeneities in the fiber.

The cast polymer rod was then machined and the desired hole pattern, which consisted of three rings of air holes in a hexagonal arrangement, was drilled into it. The preform was finally drawn to an intermediate cane, which was then sleeved with an in-house fabricated PC

#255045 Received 3 Dec 2015; revised 15 Jan 2016; accepted 17 Jan 2016; published 27 Jan 2016

tube and drawn down to fiber. A complete description of the experimental methodologies involved in the drill-and-draw technique can be found in [17]. The diameter of the final fiber was about 150 µm, whereas the core diameter was 7 µm. The average air hole diameter (d) and pitch between air holes (Λ) were 1.75 µm and 4.375 µm, respectively. The ratio d/Λ of 0.40 ensured that the mPOF was endlessly single-moded [36].

2.2 Characterization of the cast bulk PC material

The refractive index (RI) of the PC material used in our experiments was measured by using a commercially available ellipsometer VASE (J.A. Woollam), which covers a wavelength range of 210-1690 nm with a 5-nm resolution for the range 210-1000 nm and a 10-nm resolution for the range 1000-1690 nm. Figure 1(a) shows the measured material dispersion of PC and directly compares our data with other material dispersions reported in the literature. As it can be seen from Fig. 1(a), the measurements performed on PC were relatively close to the other dispersion data, with ours being slightly higher (<0.012) than the RI values from the PC datasheet [29] and Sultanova et. al. [37]. This slight difference in RI can be attributed to different preparation procedures utilized to manufacture the bulk PC material.

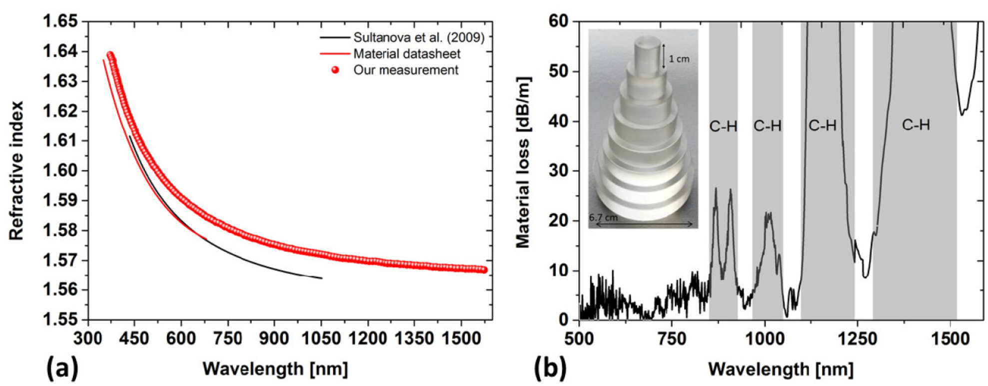

Fig. 1. (a) Material dispersion of PC. Our measurement (circles) is compared with the results of [29] (red curve) and [37] (black curve). (b) Bulk material optical loss of a PC solid rod made via casting from plastic granulates. Note the very high loss at longer wavelengths due to the absorption bands mainly caused by carbon and hydrogen bond (aliphatic and aromatic) vibrations [25,38]. Inset: PC step-like structure fabricated to measure the bulk material propagation loss.

Bulk material propagation loss was also measured within the interval 500-1600 nm based on a modified cut-back technique. A 10 cm long initial cylindrical preform was machined into an 8-step structure, with each step being 1 cm long (inset of Fig. 1(b)). We then determined the propagation loss of the material by using a broadband supercontinuum source and recording the spectrum in each step of the preform. The material loss was relatively low between 500 nm and 853 nm, as shown in Fig. 1(b). Moreover, four further transmission windows (with loss below 15 dB/m) could be detected at the wavelength ranges 876-898 nm, 917-998 nm, 1028-1102 nm, and 1247-1287 nm, respectively. The material transmission loss in the near-IR spectral range was slightly lower than the one reported in [39]. From Fig. 1(b) it may further be noticed that there is a significant amount of noise at short wavelengths. This is because of the lower loss, around a few dB/m, and also due to increasing scattering. A non-perfect surface of the sample introduces surface scattering, which is highly wavelength dependent. This leads to the growth of spectral noise towards shorter wavelengths.

2.3 Characterization of the solid-core PC mPOF

After the characterization of the bulk material we investigated the properties of the drawn mPOF. The fiber transmission loss profile was obtained via cut-back measurement. Cleaving was performed with an in-house made hot blade cleaver equipped with a flat side blade,

#255045 Received 3 Dec 2015; revised 15 Jan 2016; accepted 17 Jan 2016; published 27 Jan 2016

which yields high-quality end facets [40]. Applying the same temperature to blade and fiber, we tested several temperatures in the range 50-80°C (with steps of 5°C) so as to optimize the cleaving process for the PC mPOF. The optimal temperature of both blade and fiber was found to be 80°C. Figure 2(a) shows the transmission loss of the solid-core PC mPOF in the range of wavelengths between 550 nm and 900 nm, while Fig. 2(b) displays a microscope image of the fiber end facet with the desired hexagonal arrangement of air holes. The fiber transmission loss was found to be lower than 10 dB/m within the range 800-840 nm. Specifically, the minimum loss was 8.91 dB/m at 833.5 nm, whereas at the same wavelength the material loss was 4.37 dB/m [Fig. 1(b)]. By comparing Fig. 1(b) with Fig. 2(a) it may be noticed that the fiber loss was considerably higher than the propagation loss measured for the bulk material, especially at shorter wavelengths. This is probably due to the presence of material and geometrical inhomogeneities in the microstructured fiber. In particular, the higher loss of the PC fiber compared to its bulk material loss may arise from scattering. There are many possible sources of scattering due to the way mPOFs are manufactured [17,18,41,42]. The drilling process yields surface roughness within the holes of the polymer preform and this fact increases fiber loss. Even though the fiber drawing has the effect of smoothing the internal surface of the holes, some residual roughness in the final fiber is expected, leading to higher loss. This problem can be limited by adopting larger fiber cores [41]. Furthermore, material impurities introduced throughout the drill-and-draw process, such as dust, as well as the presence of any residual micro-swarfs on the hole surface as a consequence of the preform drilling, increase attenuation. Microbending losses, due to microdeformations in the mPOF producing scattering, are also expected. Particularly for small diameters, as is the case for the fiber characterized here, this source of loss may become important [41]. Overall it is expected that fiber loss can be substantially reduced by improving the whole PC fiber fabrication process.

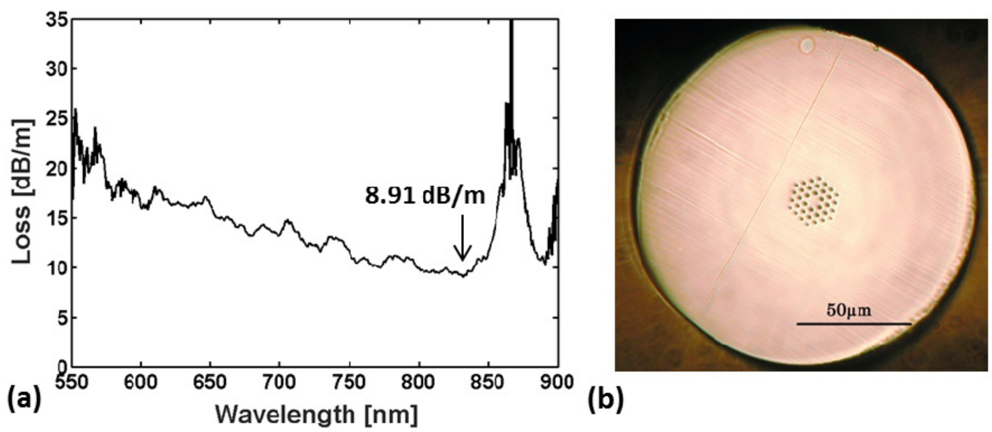

Fig. 2. (a) Transmission loss profile measured from 550 to 900 nm by the cut-back technique. The fiber was cut back from 4 m to 50 cm recording the transmission spectrum over 17 different fiber cuts. (b) Microscope image of the end facet of the solid-core PC mPOF. The fiber diameter was approximately 150 μm.

2.4 FBG inscription into the PC mPOF

The writing of the fiber Bragg grating in the polycarbonate mPOF was carried out with a 50 mW CW HeCd laser operating at 325 nm (IK5751I-G, Kimmon). For grating inscription we used the phase mask technique. The configuration of the inscription setup was the same as described in [43]. The phase mask was custom-made by Ibsen Photonics A/S. It is optimized for inscription with a HeCd laser (325 nm) and has a uniform period of 572.4 nm. The laser power was attenuated to 4 mW. The Bragg wavelength for the PC mPOF fiber was centered at 892.4 nm (with a FWHM of 0.46 nm) and the strength of the reflected peak was 25 dB, as

#255045 Received 3 Dec 2015; revised 15 Jan 2016; accepted 17 Jan 2016; published 27 Jan 2016

shown in Fig. 3. By using the RI from the material, the theoretical effective refractive index was calculated to be 1.5652 at 895.9 nm. For a pitch of 572.4 nm this gives a Bragg wavelength of 895.9 nm, which is close to the experimental value of 892.4 nm. The difference between theoretical and experimental value is due to the fact that we assumed an idealized geometry and neglected the effect of fabrication on RI in the calculation. In addition, the fiber was slightly pre-strained during the inscription process, which may lead to a mild down-shift of the FBG resonance wavelength upon release of the fiber from the inscription setup. The successful inscription of the FBG demonstrates that PC is photosensitive at typical Bragg grating writing conditions. The fiber loss at the Bragg grating wavelength (892.4 nm) was 11.37 dB/m [Fig. 2(a)]. However, transmission loss did not represent a critical factor in our experiments as only short lengths of the fiber were used. Although the laser power was only 4 mW, the FBG writing took just a few minutes. The inscription process was fast considering that the fiber was dopant-free. In particular, without the use of dopants the fastest writing time in PMMA mPOFs by means of a HeCd laser was shown to be slightly below 7 minutes in [43] (the laser power was 30 mW). For PC mPOFBGs, the average inscription time with a HeCd laser is about 6 minutes at a power of 4 mW. Short inscription times are of importance for the stability of a grating. The writing time in PMMA mPOFs can be reduced by either doping the fiber core [8,44,45] or using a different laser [46]. The same should hold true also for PC.

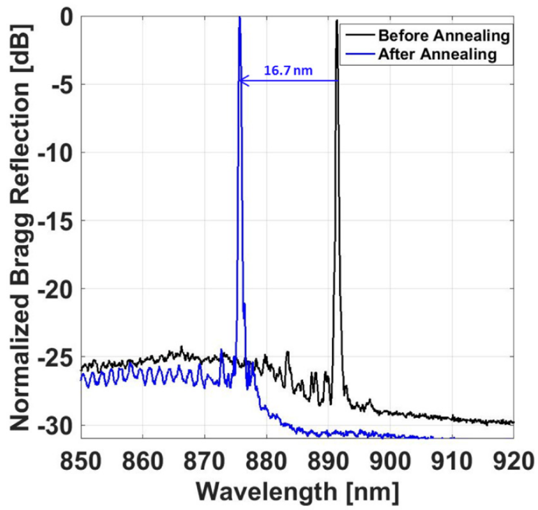

Fig. 3. PC mPOFBG spectrum at room temperature before annealing (black) and after annealing (blue).

The fiber was then annealed in order to improve the stability of the strain sensing [34,47]. Specifically, the annealing was done in two phases. First at 120°C for 24h, after which the resonance wavelength was 881.7 nm (10.7 nm lower than that of the un-annealed FBG). Then at 130°C for 12 h, which further blue-shifted it by 6.0 nm. After annealing the new Bragg wavelength was thus centered at 875.7 nm, with a total blue-shift of 16.7 nm (Fig. 3). The shift in the resonance wavelength was probably caused by fiber shrinkage [34], due to (at least partial) relaxation of the polymer chains as a consequence of the annealing process [48].

2.5. Strain and temperature sensing with the PC mPOFBG

The FBG was characterized in terms of sensitivity to strain and temperature by using a fiber coupler, a supercontinuum source (SuperK Compact by NKT Photonics A/S) and an optical spectrum analyzer (OSA, Ando AQ6315A). The two ends of the PC mPOF were glued to two micro-translation stages, one of which being fixed and the other one free to move according to the applied axial strain. The fixed end was butt-coupled to a silica step-index fiber through

#255045 Received 3 Dec 2015; revised 15 Jan 2016; accepted 17 Jan 2016; published 27 Jan 2016

which light was launched into the fiber. The axial strain values were calculated as the ratio (expressed in %) of the change in the length between the two gluing points ΔL to the original length of the fiber L_0 (4 cm). To minimize time-dependency in the mechanical behavior, the FBG reflection spectrum was read after approximately 10 minutes each time the axial strain was varied. The fiber was gradually stretched up to 3% (loading phase, "forward") and then the strain was slowly decreased until the original dimension was recovered (unloading phase, "reverse"). Figure 4(a) displays the results from the strain tuning of the PC FBG in forward and reverse straining. The Bragg wavelength exhibited a linear response over the strain range 0-3%, with a sensitivity of 0.701 ± 0.003pm/με calculated by linear regression. This sensitivity is very close to the value of 0.71 pm/με reported for PMMA 3-ring mPOFBGs at 850nm [49] and 827nm [50], and similar to that of 0.64 pm/με measured for a TOPAS 2-ring mPOFBG at 870 nm [13]. Moreover, the fiber did not show any hysteresis in the unloading phase, since the forward and reverse curves were perfectly overlapped, as shown in Fig. 4(a). Indeed, the strain sensitivity in the reverse phase was calculated to be still the same as the forward one (namely, 0.701 ± 0.003pm/με).

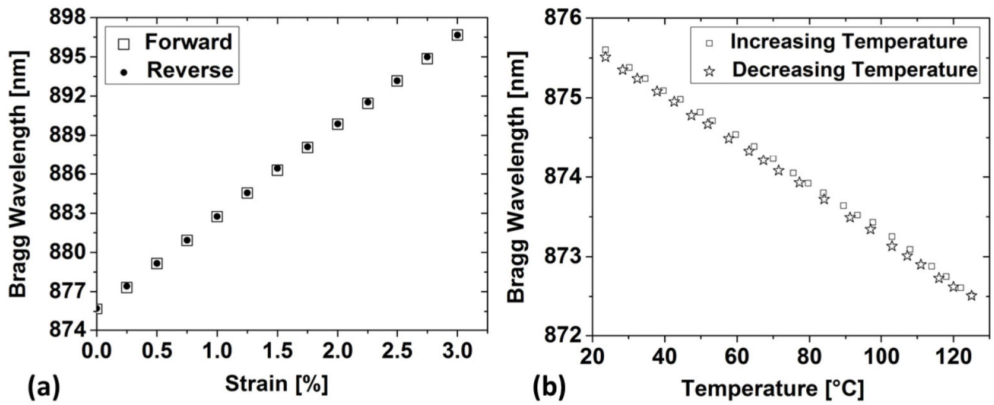

Fig. 4. (a) Strain response of the PC mPOFBG at room temperature. (b) Temperature response of the unstrained PC mPOFBG.

The temperature response of the solid-core PC mPOFBG was also investigated. The setup was similar to the one used for strain measurements, except for the Bragg grating now being placed on a resistive hot stage so as to control its temperature. A thermocouple with an uncertainty of around 0.3°C was placed as close as possible to the PC mPOF. Several layers of lens paper were used to cover it and therefore obtain a more uniform temperature. Each Bragg grating wavelength was recorded after 15 minutes once a new temperature value was set. Figure 4(b) shows the temperature tuning of the PC mPOFBG performed in a forward-backward test. The PC mPOFBG displayed a linear response between room temperature (23.6°C) and 125°C, showing a negative Bragg wavelength shift with increasing temperature. No malfunctioning was observed even at the highest temperatures. Note that in a study of the temperature response of FBGs inscribed in a PMMA 4-ring mPOF [34] with a similar diameter as the one of our PC fiber, a time interval of 10 minutes before readings were taken at each measurement step was sufficient to observe a markedly non-linear response when the elevated temperature region was approached.

The maximum temperature applied in our characterization of the PC grating (125°C) was greater than the one previously demonstrated by using a high-T_g TOPAS mPOFBG (110°C) [14], and well above the maximum operational temperature of PMMA (92 °C) reported in [34]. Furthermore, the PC mPOFBG response was seen to be linear in the cooling-down test. From a linear regression over the whole temperature range, the sensitivity of the FBG was calculated to be equal to −29.99 ± 0.17 pm/°C in the forward test and to −29.78 ± 0.09 pm/°C in the backward test. No significant hysteresis was observed as the temperature was ramped down, as also confirmed by the almost unaltered sensitivities. The stability of the fiber was

#255045 Received 3 Dec 2015; revised 15 Jan 2016; accepted 17 Jan 2016; published 27 Jan 2016

expected mainly for two reasons. The first one was that the T_g of the PC used in the present study is 20°C higher than the maximum operational temperature demonstrated here. This margin can be thought of as the minimum one to ensure long-term stability of a POFBG [14]. Secondly, the combination of two distinct annealing phases at 120°C and 130°C was likely to have significant impact in this regard, as early investigations showed the annealing process to considerably contribute to enhancing the thermal stability of polymeric FBGs and extending the linearity in their response to temperature [34,47]. The particular temperature of 125°C makes PC POFBGs applicable to certain areas of automation technology and automotive engineering. For instance, in the engine compartment of a vehicle, temperatures can go up to 125°C [27]. Polycarbonates make this area now accessible to polymer-based FBGs for the first time to our knowledge. In addition, PC can be sterilized with steam autoclaving [28], though for limited reuse applications. Autoclaves for sterilization typically work at 121°C for 15-20 minutes. No previous POFBG could withstand such conditions. The latter characteristic can be of great importance from a biomedical perspective.

It should also be mentioned that PC is not humidity-insensitive. An example of polymers used for manufacturing humidity-insensitive mPOFBGs is TOPAS [13]. As a reference, the percent water absorption of PC is 0.12% in air at 23°C and 50% relative humidity (RH) (generally measured after 24 h), whereas this value increases up to 0.3% (at saturation) when the PC is immersed in distilled water at 23°C [29]. Since the PC mPOFBG characterization was carried out in the open laboratory, its response to temperature could have been affected by cross-sensitivity to humidity. The true temperature and humidity responses of the PC mPOFBG, as assessed in a humidity-controlled environment (i.e., by using a climate chamber), are out of the scope of this paper.

2.6 Mechanical testing of the PC mPOF

The datasheet by the manufacturer of the used PC reports a tensile modulus of 2.35 GPa, a strain at break >50%, and yield stress and strain of 63 MPa and 6.0% [29], respectively. The tensile strain (%) is defined as $\varepsilon = 100 \cdot (l - l_0)/l_0$, where l_0 represents the initial length of the sample and l denotes the instantaneous length of the sample being stretched. All the data presented here are based on the engineering stress defined as $\sigma = F/A_0$, with A_0 being the initial cross sectional area of the sample and F the stretching force. Note that the structuring of the polymer in the direction of the drawing due to the specific drawing conditions applied in the fiber fabrication process can affect the strain-stress behavior [48,51]. Moreover, tensile test results may also depend on the test temperature [52] and applied strain rate [2,48], as well as on the specific RH value (as water can act as a plasticizer of polymer materials), where the latter factor is expected not to be important for humidity-insensitive fibers, such as TOPAS. We carried out a tensile test on an un-annealed PC 3-ring microstructured optical fiber using an in-house built tensile testing machine. Five fiber samples were tested at a constant straining rate of 66%/min in a monitored open environment (T = 21.9-23.7°C, RH = 34.0-48.1%). The average diameter of the fiber samples was 146 ± 4 μm. The diameter measurements were performed with a micrometer screw gauge and cross-checked by means of an optical microscope. Both methods led to values in reasonable agreement. The cross-sectional area of the air holes in the microstructured region was neglected, as it accounted only for about 0.5% of the whole fiber cross section. Figure 5 shows a typical engineering stress-strain curve of the tested PC fiber samples. This kind of representation is useful as it contains more information than that presented in the datasheet. It may indeed be seen from Fig. 5 that our PC mPOF did not show a distinct yield point based on the Considere's construction method [53], as $d\sigma/d\varepsilon$ continued to be positive, although its value became considerably low at strains around 5%. After a further 10% elongation region at nearly constant stress, the fiber exhibited significant strain hardening at high strains (>15%) where the molecular alignment stiffened the drawn polymer.

Figures 6(a) and 6(b) summarize the results expressed in terms of Young's modulus (E) and break point, respectively. We calculated the Young's modulus using linear regression of the stress-strain data within the strain region of 0.05%-0.25%, as recommended in ISO 527-

#255045 Received 3 Dec 2015; revised 15 Jan 2016; accepted 17 Jan 2016; published 27 Jan 2016

1:1996 for plastics in tension. The Young's modulus of the PC mPOF was estimated to be equal to 3.03 ± 0.10 GPa. This is approximately 35% larger than the value reported in the bulk material datasheet [29]. Notice that thermal annealing commonly has the effect of lowering E and increasing ductility [48,51]. The curve shape is also likely to change as a result of the annealing process [48].

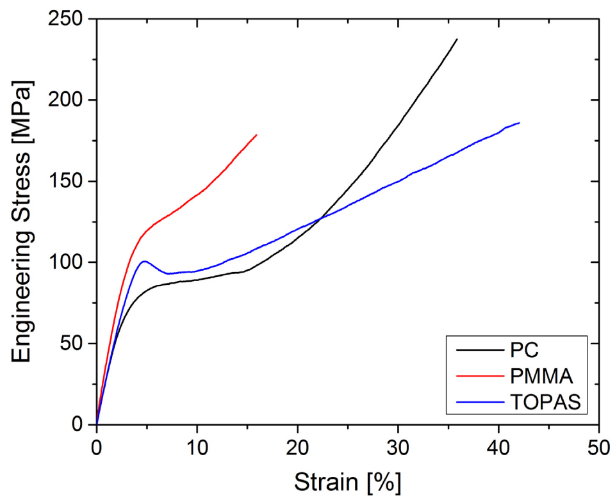

Fig. 5. Typical stress-strain curves of 3-ring solid-core PC, PMMA, and TOPAS mPOFs with an average diameter 146 ± 4 μm, 141 ± 5 μm, and 133 ± 4 μm, respectively. Average diameter estimation for 5 samples of each fiber was performed by adopting a confidence interval (CI) of 95%.

Figures 5, 6(a), and 6(b) further include the data from the experiments carried out on un-annealed GEHR PMMA [54] and TOPAS 8007S-04 [55] 3-ring mPOFs, which were tested in extension for comparison. The average diameters of the PMMA and TOPAS fibers were 141 ± 5 μm and 133 ± 4 μm, respectively. Similar drawing conditions as for the PC mPOF were also applied.

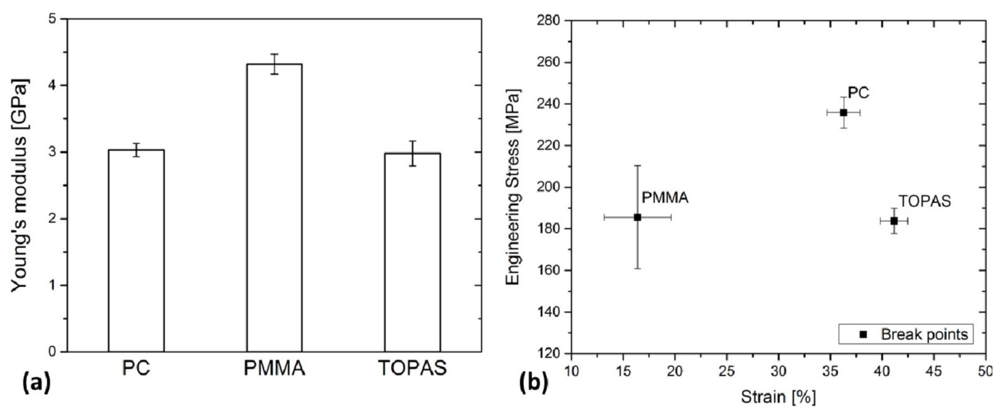

Fig. 6. (a) Average Young's moduli calculated on the whole statistical group (5 samples of each fiber). The bars represent a CI of 95%. (b) Average break points (the bars indicate a CI = 95%).

The stress-strain curves measured for the TOPAS mPOF exhibited a drop in the stress (usually identified as the yield point [53]) after the quasi-linear region, whereas the PMMA mPOF did not. These measurements displayed a similar increase in Young's modulus as the PC fiber compared to the data reported by the respective manufacturers. Indeed, the average E

#255045 Received 3 Dec 2015; revised 15 Jan 2016; accepted 17 Jan 2016; published 27 Jan 2016

values of PMMA and TOPAS were found to be 4.32 ± 0.15 GPa (34% greater than in [54]) and 2.98 ± 0.19 GPa (+ 15% compared to the company's datasheet [55]), respectively. The PC tensile strain at break was 36.3 ± 1.6%, slightly lower than TOPAS (41.2 ± 1.3%) but more than twice as much as PMMA (16.4 ± 3.2%). Note that a higher strain at break basically means a larger strain range available before failure. In addition, as a result of the higher degree of strain hardening, the PC mPOF could bear an average tensile stress at break of 235.9 ± 7.4 MPa, which is considerably greater than those measured for PMMA (185.5 ± 24.8 MPa) and TOPAS (183.8 ± 6.1 MPa).

A replacement of PMMA with PC-based mPOFBGs in strain sensing would increase the maximum operative temperature from 90°C to at least 125°C. Moreover, the lower Young's modulus of PC compared to PMMA is likely to increase the sensitivity of PC-based mPOFs in vibration sensors and accelerometers [56].

3. Conclusion

In this paper we have presented the fabrication of an FBG sensor in a PC mPOF manufactured through a multistage process starting from plastic granulates. The solid-core PC mPOF was characterized optically as well as mechanically. We observed fiber loss below 10 dB/m within the wavelength range 800-840 nm, with a minimum of 8.91 dB/m at 833.5 nm. In the mechanical characterization, the solid-core PC mPOF showed a pseudo-yield point after being strained by about 5%, and had relatively low Young's modulus and high strain at break compared to PMMA.

Furthermore, we reported for the first time that an FBG can be UV-written in a PC fiber. The FBG was inscribed in only a few minutes at a power of 4 mW. This inscription time was extremely fast considering that the fiber was undoped. Most importantly, we have demonstrated strain sensing up to 3% in a PC FBG, and a linear response of the grating to temperature up to 125°C, which is, to our knowledge, the currently highest reported operating temperature for a POFBG. We do think that PC FBGs represent a step towards the development of a reliable high-temperature-resistant polymer-based FBG technology.

Acknowledgments

The research leading to these results has received funding from the People Programme (Marie Curie Actions) of the European Union's Seventh Framework Programme FP7/2007-2013/ under REA grant agreement n° 608382. The authors also acknowledge Financial support from Innovation Fund Denmark for the project ShapeOCT (J. No. 4107-00011A). C.M. acknowledges support from Danish Council for Independent Research (FTP Case No. 4184-00359B). A.S. acknowledges the Eugen Lommel Stipend for financial support.

#255045 Received 3 Dec 2015; revised 15 Jan 2016; accepted 17 Jan 2016; published 27 Jan 2016